Biomedicine & Pharmacotherapy 124 (2020) 109927

Contents lists available at ScienceDirect

Biomedicine & Pharmacotherapy

journal homepage: www.elsevier.com/locate/biopha

Doxorubicin and α-Mangostin oppositely affect luminal breast cancer cell stemness evaluated by a new retinaldehyde-dependent ALDH assay in MCF-7 tumor spheroids

Irene Bissoli, Claudio Muscari*

Department of Biomedical and Neuromotor Sciences (DIBINEM), University of Bologna, Bologna, Italy

ARTICLE INFO

Keywords:
Doxorubicin
α-mangostin
Aldehyde dehydrogenase
Cancer stem cell
MCF-7
Breast cancer

ABSTRACT

According to cancer stem cell theory, only a limited number of self-renewing and cloning cells are responsible for tumor relapse after a period of remittance. The aim of the present study was to investigate the effects of Doxorubicin and α-Mangostin, two antiproliferative drugs, on both tumor bulk and stem cells in multicellular tumor spheroids originated from the luminal MCF-7 breast cancer cell line. A new and original fluorimetric assay was used to selectively measure the activity of the retinaldehyde-dependent isoenzymes of aldehyde dehydrogenase (RALDH), which are markers of a subpopulation of breast cancer stem cells.

The administration of 5 μg/ml (12.2 μM) α-Mangostin for 48 h provoked: i) a marked disaggregation of the spheroids, leading to a doubling of their volume ($p < 0.01$), ii) a 40 % decrease in cell viability ($p < 0.01$), evaluated by the acid phosphatase assay, and iii) a reduction by more than 90 % of RALDH activity. By contrast, Doxorubicin given for 48 h in the range of 0.1–40 μM did not significantly reduce cell viability and caused only a modest modification of the spheroid morphology. Moreover, 40 μM Doxorubicin increased RALDH activity 2.5-fold compared to the untreated sample. When the two drugs were administered together using 5 μg/ml α-Mangostin, the IC_{50} of Doxorubicin referred to cell viability decreased six-fold and the RALDH activity was further reduced. In conclusion, the combined administration of Doxorubicin and α-Mangostin provoked a significant cytotoxicity and a remarkable inhibition of RALDH activity in MCF-7 tumor spheroids, suggesting that these drugs could be effective in reducing cell stemness in luminal breast cancer.

1. Introduction

New pharmacological strategies need to be adopted to prevent tumor relapses. According to the cancer stem cell (CSC) theory [1], only a few of these cells can be responsible for the recurrence of the tumor after a period of remittance. Unlike the cells of the tumor bulk, CSCs better resist treatments and move from the primary site to produce metastases. The presence of CSCs in the tumor mass has often been considered an unfavorable prognostic event [2].

In breast carcinoma three main populations of CSCs have been identified: $CD44^+/CD24^{-/low}$ CSCs, CSCs showing an elevated activity of aldehyde dehydrogenase ($ALDH^+$ CSCs), and the very poorly represented, but extremely tumorigenic, $CD44^+/CD24^{-/low}/ALDH^+$ CSCs [3]. The ALDH superfamily consists of $NAD(P)^+$ dependent enzymes that catalyze the oxidation of endogenous and exogenous aldehydes to the corresponding carboxylic and CoA-ester acids [4]. Aldehydes are formed during the metabolism of alcohols, amino acids, vitamins, retinoids, steroids and lipid peroxides, and since they are strong electrophilic compounds with terminal carbonyl groups, they may be involved in the synthesis of adducts with proteins and nucleic acids that cause serious adverse biological effects [5]. These enzymes are also involved in the metabolism of reactive oxygen species (ROS) and in drug resistance [6]. The study of Liu et al. on breast carcinoma [7] shows that $CD44^+/CD24^{-/low}$ CSCs can differentiate into $ALDH^+$ CSCs, while the inverse process may also occur. Moreover, this work demonstrates the feasibility of a parallel and bidirectional epithelial-mesenchymal and mesenchymal-epithelial transition. These two sub-populations of CSCs are distributed in different regions of the tumor, since $CD44^+/CD24^{-/low}$ cells are located on the invasive front while the $ALDH^+$ cells are more frequently found in the central area. Furthermore, there is a high frequency of $CD44^+$/CD24- cells in basal-like breast carcinomas, whereas $ALDH^+$ cells are mainly present in luminal carcinomas.

In this study, we used a new and original assay of ALDH to measure the activity of retinaldehyde-dependent dehydrogenase isoenzymes,

* Corresponding author at: Via Irnerio, 48, 40126 Bologna, Italy.
E-mail address: claudio.muscari@unibo.it (C. Muscari).

https://doi.org/10.1016/j.biopha.2020.109927
Received 19 July 2019; Received in revised form 29 December 2019; Accepted 29 December 2019

here abbreviated as RALDH, since they seem to be specific markers of CSCs in many tumors [8]. In particular, luminal breast CSCs are often selected by ALDH1A1 (RALDH1A1) and ALDH1A3 (RALDH1A3) [9].

We investigated the effects of Doxorubicin and α-Mangostin (α-MG), two antiproliferative drugs, in a three-dimensional (3D) model of breast cancer, by comparing their toxicity against bulk cells with that exerted towards RALDH$^+$ CSCs. α-MG is a natural xanthone able to counteract the malignancy of several types of cancer, including prostate, breast, pancreas, colon, skin and lung carcinomas, by affecting all phases of carcinogenesis: initiation, promotion and progression [10]. Different molecular mechanisms were attributed to α-MG, including cell apoptosis and cell cycle arrest. α-MG also inhibits cell migration/invasion and the process of angiogenesis. Doxorubicin belongs to the family of anthracyclines and causes both the arrest of cell growth and cell death [11]. It generates reactive oxygen species (ROS) and, by damaging mitochondria, provokes the release of cytochrome c and cell apoptosis [12]. Indeed, Doxorubicin preferentially binds cardiolipin, a component of the inner mitochondrial membrane, leading to an impairment of the electron transport chain and oxidative phosphorylation [13]. In addition, Doxorubicin binds nuclear DNA strands, impeding transcription cell division. It also forms a DNA inhibiting complex with topoisomerase II that affects DNA replication and induces cell apoptosis [14].

Through this research, we demonstrated how effective the inhibitory effect of α-MG was on RALDH activity in multicellular tumor spheroids (MCTSs) originated from MCF-7 breast cancer cells. On the contrary, Doxorubicin increased RALDH activity in MCTSs. When both drugs were administered contemporarily, the overall cytotoxic effect increased and the RALDH activity was almost completely blunted, suggesting that the combination of these drugs could significantly improve the therapeutic efficacy of Doxorubicin.

2. Materials and methods

2.1. Culture condition for breast adenocarcinoma cell lines

Chemicals were purchased from Sigma-Aldrich (St. Louis, MO, USA), unless otherwise stated. The luminal MCF-7 and triple negative MDA-MB-231 breast adenocarcinoma cell lines [ECACC, Sigma-Aldrich] were used for the study. After thawing from liquid nitrogen, they were seeded on petri dishes and used for the experiments after a week. The complete culture medium consisted of Dulbecco's Modifed Eagle's Medium (DMEM) with supplementary 100 U/ml penicillin, 100 μg/ml streptomycin, and 10 % fetal bovine serum (FBS). The cells were put in an incubator at 37 °C with 5 % CO_2 and the medium was replaced every 2–3 days. Upon reaching semiconfluence, the cells were detached with 0.05 % trypsin in 0.53 mM EDTA and seeded at a lower density for cell expansion.

2.2. Production of MCTSs

The protocol used for MCTS generation was that described by Scolamiero et al. [15] with some modifications. Briefly, MCF-7 cells were detached by trypsin/EDTA digestion, centrifuged at 800 x *g* for 8 min, and resuspended with a stem cell-enriching medium containing DMEM/F12 (1:1) supplemented with 100 U/ml penicillin, 100 μg/ml streptomycin, 20 ng/ml epidermal growth factor (EGF), 10 ng/ml basic fibroblast growth factor (FGF-b), and 2 % B27 (ThermoFisher Scientific, Waltham, MA, USA). Cells were counted by a Bürker chamber and 5×10^3 cells/well were seeded in ultra-low attachment (ULA) 96-well round-bottomed plates Corning B.V., Life Sciences, Amsterdam, The Netherlands in 200 μl of the medium. Cells were gathered in the center of the well by centrifugation at 1000 x *g* for 10 min. They were then incubated at 37 °C for 72 h to generate compact MCTSs, spherical in shape and surrounded by well-defined edges.

2.3. Evaluation of MCTS morphology

Phase-contrast images of MCTSs were observed using an inverted microscope (IX50, Olympus Italia, Segrate, Italy), captured by a Canon G16 camera (Canon Europa, Amstelveen, The Netherlands), and imported into Image-J software (Fiji, http://fiji.sc/). The border of each spheroid was manually drawn to obtain the shape and related magnitude of the pseudo-circular area (A). The average radius (r) was then calculated through the formula: $r = \sqrt{A/\pi}$ and used to obtain the volume value (V) with the formula: $V = 4/3\ \pi\ r^3$.

2.4. Measurement of cell viability in MCTSs

Cell viability was determined by measuring the activity of acid phosphatase (APH), according to the method of Friedrich et al. [16] with some modifications. Briefly, the multiwell plate containing MCTSs was centrifuged at 800 x *g* for 10 min, 150 μl of the supernatant were removed from each well, and the pellet washed with the same volume of PBS. A second centrifugation at 800 x *g* for 10 min was repeated and 100 μl were discarded. Then, 0.4 mg p-nitrophenylphosphate and 0.1 % TritonX in 100 μl of 90 mM citrate buffer solution, pH 4.8, were added to each well containing a single MCTS. The plate was incubated at 37 °C for 90 min and the enzyme reaction was interrupted with 20 μl 1.0 M NaOH. Finally, the absorbance was read at 405 nm using the Victor2 multiwell plate reader (Perkin Elmer, Milan, Italy).

The summation effect of Doxorubicin plus α-MG on cell death was also investigated. This was performed by calculating the ratio between the measured cytotoxicity of the two drugs administered together and their expected cytotoxicity, which is the mathematical sum of the individual drug cytotoxicity [17,18]. A measured cytotoxicity higher than the expected values, i.e. measured/expected (M/E) ratio > 1.0, indicates a synergistic effect. Consequently, the M/E ratio < 1.0 shows an antagonistic effect and equal to 1.0 an additive interaction [19].

The trypan blue exclusion assay was also performed to measure the percentage of living and dead cells after their isolation from MCTSs obtained by trypsin/EDTA digestion. Carboxyfluorescein diacetate succinimidyl ester (CFSE, Invitrogen, Waltham, MA, USA), at a concentration of 0.1 μg/ml, was used as a fluorophore to identify viable cells after their seeding on ULA wells and following centrifugation.

2.5. Assay of RALDH activity

The retinaldehyde-dependent activity was firstly determined using a purified extract of bread yeast ALDH (1 U/mg) to verify some basic parameters, including the solubility of all trans-retinal in the assay solution and the kinetics of NAD$^+$ reduction. Concentrations in the range of 0.01-0.1 mg/ml for ALDH, 20–200 μM for all trans-retinal in dimethylsufoxide (DMSO), and 0.4 − 4 mM for NAD$^+$ were tested using PBS at pH 7.0, or 50 mM HEPES at pH 8.0, as buffer solutions. The kinetics was detected at 340 nm using the Jasco V-530 spectrophotometer and expressed as μmoles NADH min^{-1} μg $protein^{-1}$. Once the best concentration of the reagents was established for the photometric assay, its adaptation to a more sensitive fluorimetric assay was performed and applied to detect the RALDH activity. MCF-7 and MDA-MB-231 cell monolayers, as well as pools of 40 MCF-7 spheroids, were dissociated by trypsin/EDTA digestion. The cell suspensions were then centrifuged at 800 x *g* for 8 min and, after removing the supernatant, a hypotonic shock was performed with 100 μl bidistilled water at 37 °C for 15 min. Then, the samples were centrifuged at 12,000 x *g* for 10 min, the supernatant was collected and 10 μl were used to measure the protein concentration with the Bredford assay [20]. The remaining supernatant was immediately used to perform the assay of RALDH activity in a 96 mutiwell plate. The final composition in 100 μl of 50 mM HEPES at pH 8.0 was: 80 μM all trans-retinal, 25 μg/ml resazurine, 5 mM NAD$^+$, and 40 μl sample. Each analysis was carried out in duplicate. The assay without NAD$^+$ served to measure the background signal. The fluorescence detection of the NADH dependent reduction of resazurine to resorufine was followed by the

Table 1
Forward (F) and Reverse (R) primer sequences.

Gene	Sequence
ALDH1A1_F	AGCAGGAGTGTTTACCAAAGA
ALDH1A1_R	CCCAGTTCTCTTCCATTTCCAG
ALDH1A2_F	TTGGTTCAGTGTGGAGAAGG
ALDH1A2_R	AAAGCTTGCAGGAATGGTTTG
ALDH1A3_F	CTTCTGCCTTAGAGTCTGGAAC
ALDH1A3_R	CGTATTCACCTAGTTCTCTGCC
ALDH1B1_F	CCCAAGCGTGATCCTGAAC
ALDH1B1_R	ATGTCTGGGTTCAGAATGGG
ALDH1L1_F	TTGAGCTGACAGAGGCAGAG
ALDH1L1_R	CTCCACCAGCCTCACAACG
ALDH1L2_F	AAAGGTCGTGAGGAAACTGAG
ALDH1L2_R	TTCCATCGTCTGCATCTGTG
ALDH2_F	ATGAGTTTGTGGAGCGGAG
ALDH2_R	TTCCCCGTGTTGATGTAGC
ALDH3A1_F	TGCTACGTGGACAAGAACTG
ALDH3A1_R	CACAATTTGGTTCTGGATCGAG
ALDH8A1_F	AAAGTCGGCATTCCCTCTG
ALDH8A1_R	CAACTTATCCACTCCCTCACC
GUSB_F	AGGTGATGGAAGAAGTGGTG
GUSB_R	AGGATTTGGTGTGAGCGATC
HPRT1_F	AGATGGTCAAGGTCGCAAG
HPRT1_R	GTATTCATTATAGTCAAGGGCATATCC
β-actin_F	ACCTTCTACAATGAGCTGCG
β-actin_R	CCTGGATAGCAACGTACATGG

VICTOR^2 multi-plate reader set at 530 nm excitation and 590 nm emission wavelengths and at a constant temperature of 25 °C.

2.6. RT-PCR of ALDH isoenzymes

The quantitative analysis of ALDH1A1, ALDH1A2, ALDH1A3, ALDH1B1, ALDH1L1, ALDH1L2, ALDH2, ALDH3A1 and ALDH8A1 transcripts was performed by Real-Time PCR (RT-PCR). The amount of mRNA of each isoenzyme present in the MCTSs was calculated as $2^{-\Delta\Delta Ct}$ [21] in relation to the corresponding value obtained in cell monolayers, which was normalized to 1.0.

Total RNA was extracted with TRIzol (Invitrogen) and 1 μg RNA was used for reverse transcription, which was performed with the RNA-to-cDNA kit (Applied Biosystems, Forster City, CA, USA).

Primer sequences (Table 1) were identified through the website of the Integrated DNA Technologies company. Primers were also validated in the hepatocarcinoma lines HepG2 and Huh-7. Among the three reference genes that were evaluated (GUSB, HPRT, β-actin), we chose GUSB because its values remained stable (data not shown) and its expression does not substantially change under hypoxia conditions [22]. The amplification reactions were performed in triplicate in the presence of the SYBR Green probe (BioRad, Hercules, CA, USA) and the iTaq Universal SYBER Green Supermix (BioRad). The analysis was performed using the Icycler thermal cycler (BioRad) driven by the iCycler iQ Detection System Version 3.0 software (BioRad).

A semi-quantitative analysis of the mRNA of ALDH isoenzymes was also carried out to compare their expression in each sample, assuming that mRNA concentrations were inversely correlated to the corresponding Ct values.

2.7. Statistical analysis

Statistical analysis was performed using the software GraphPad Prism version 4.0 (San Diego, CA, USA). Values were expressed as mean ± SEM. One-way analysis of variance (ANOVA) followed by Bonferroni's or Dunnett's post-hoc test was used for multiple comparisons. The Student's *t*-test for unpaired data was used when only two coupled averages were analyzed. IC_{50} concentrations with the corresponding correlation coefficient (R^2) were calculated using the nonlinear regression analysis of cell viability data. Statistical significance was assumed for $p \leq 0.05$.

3. Results

3.1. Optical features of MCTSs

MCF-7 cells were seeded in each well at the fixed amount of 5×10^3 cells. After centrifugation, they formed a homogeneous layer on the concave bottom of the ULA well. Cell uptake of the vital dye CFSE

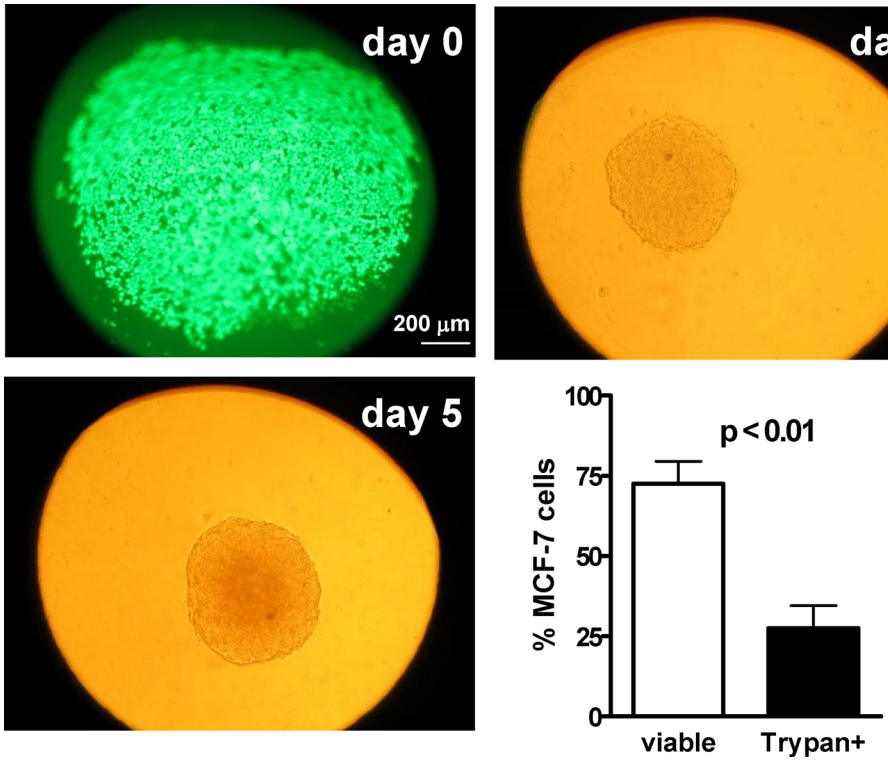

Fig. 1. MCTS production and cell viability. MCF-7 cells were seeded at a density of 5×10^3 per well in ULA 96-well round-bottomed plates. A representative microscopy field shows the CFSE vital staining present in all cells just after their seeding (day 0). Cells began to aggregate and after 72 h generated an MCTS (day 3) which grew for another 48 h (day 5). The bar graph shows the percentage of viable and dead cells (Tripan$^+$) in MCTSs at day 5, as mean ± SEM of 4 separate experiments. Statistics were performed by Student's t-test.

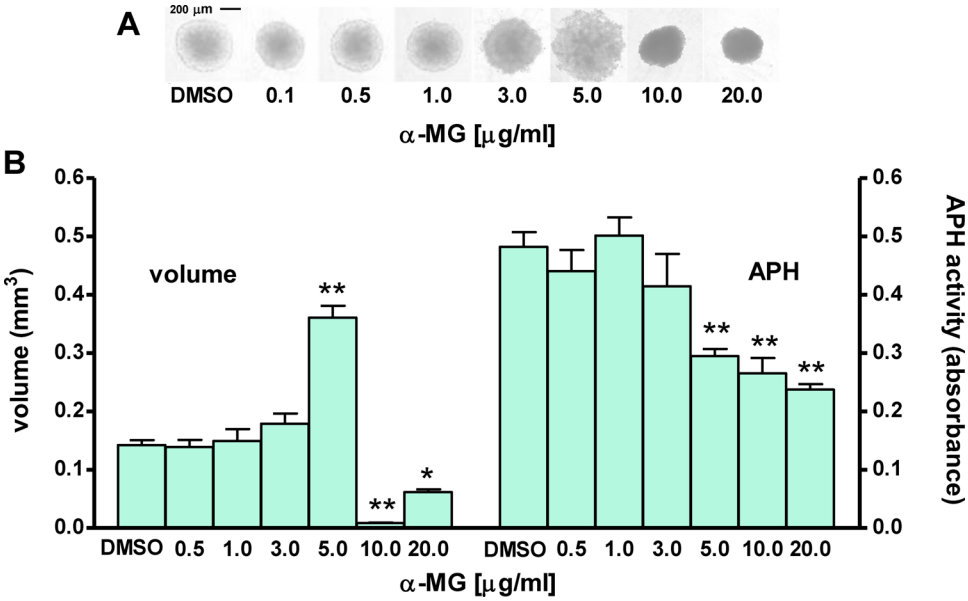

Fig. 2. Morphology and APH activity of MCTSs treated with α-MG.
A. Three and 5 µg/ml α-MG provoked both disaggregation and surface irregularity of MCTSs. Concentrations of 10 and 20 µg/ml led to a homogeneous increase of MCTSs density as a sign of diffused cell damage. B. The volume of MCTSs significantly increased with 5 µg/ml α-MG, in relation to the untreated spheroids (DMSO), as a consequence of cell detachment. Higher and more toxic concentrations instead reduced the size of MCTSs. According to the observed changes in MCTS morphology, a significant decrease in APH activity occurred in the presence of 5 µg/ml α-MG or higher concentrations. Values are means ± SEM of 4 separate experiments, each obtained in duplicate. ANOVA was followed by Dunnett's test. *$p < 0.05$ and **$p < 0.01$ vs the corresponding value of DMSO.

confirmed their viability (Fig. 1). Three days later, the cells were aggregated as a 3D spheroid with a well defined edge. The increasing density that could be observed from the periphery to the center of the spheroid was due to 3D cell overlapping. At day 3, the average diameter of MCTSs was 554 ± 24 µm, a size that provokes hypoxia in the center of the spheroid [23]. At day 5, the diameter increased, reaching 646 ± 25 µm. At this time, the internal density of each spheroid was more accentuated and the percentage of cell death, evaluated by the trypan blue staining, was 27.5 ± 7.0 (Fig. 1).

3.2. Morphology and viability of MCTSs treated with α-MG

MCTSs were treated with α-MG in the range of 0.5 – 20 µg/ml for 48 h. No morphological changes occurred at the lowest concentrations (Fig. 2A). An initial damage was shown with 3 µg/ml, which caused a diffuse increase in the density of the spheroid and made its edge irregular. The concentration of 5 µg/ml provoked a more toxic effect with evident signs of MCTS disaggregation that augmented its volume (Fig. 2B) and decreased its density, while the spheroid surface became extremely indented. A drastic change of morphology was observed again with 10 and 20 µg/ml, which reduced the spheroid to a dark compact mass of smaller size. Cell viability, measured as APH activity, decreased in a dose-dependent manner and was significantly reduced to about 50 % with 5, 10 and 20 µg/ml (Fig. 2B).

3.3. Effects of Doxorubicin and Doxorubicin plus α-MG on MCTS morphology and viability

Doxorubicin was administered to MCTSs in the range of 0.1–40 µM for 48 h. At 5 µM the edge of the spheroids acquired an irregular and jagged shape (Fig. 3A). These changes were more pronounced at higher concentrations, suggesting the occurrence of a dose-dependent effect of Doxorubicin on MCTS dissociation. This was confirmed by the progressive increase in volume starting from 5 µM (Fig. 3B).

The contemporary administration of 5 µg/ml α-MG provoked a biphasic trend of volume modification in the MCTSs treated with 0.1–40 µM Doxorubicin for 48 h. At 0.1 µM Doxorubicin, the increase in volume was almost completely due to the presence of α-MG, which led to the above-mentioned marked disaggregation of the spheroid. By contrast, with 0.5 and 1 µM Doxorubicin, the spheroid size was only slightly augmented, due to the combinatory effect of the two drugs that significantly reduced the number of viable cells (Fig. 3B-C). The volume of MCTSs increased again when α-MG was administered with Doxorubicin ranging from 5 to 40 µM, as a consequence of the synergic effect of the two drugs on MCTS dissociation.

With regards cell viability, Doxorubicin alone did not provoke any significant changes at all doses tested (Fig. 3C). Only a decreasing trend of cell viability with increasing Doxorubicin concentrations was observed, but without reaching statistical significance (Fig. 3D). By contrast, α-MG plus Doxorubicin caused a significant and dose-dependent reduction in cell viability (Fig. 3C, D).

The percent change in MCTS cell viability compared to the untreated samples was used to measure the IC_{50} of each drug or the IC_{50} of Doxorubicin in the presence of 5 µg/ml α-MG (Table 2). MCTSs were particularly resistant to Doxorubicin, but very sensitive to α-MG, as shown by the values of IC_{50}, which were 50.5 mM and 29.7 µM, respectively. By treating MCTSs with 5 µg/ml α-MG and increasing doses of Doxorubicin, the IC_{50} of the latter was reduced to 8.7 mM.

The injury provoked by the combined treatment was additive and not synergistic, as the M/E ratio, calculated using concentrations of 12.2 µM for both drugs, was 1.03 (approximately equal to 1.0) (Table 2). The same M/E ratio was obtained using 2.44 µM Doxorubicin and α-MG (data not shown).

3.4. Characterization of RALDH activity assay in cell monolayers and MCTSs

The kinetics of NADH production by a purified extract of bread yeast ALDH is shown in Fig. 4A. All trans-retinal was used as a substrate to detect the activity of RALDH isoenzymes. The optimal concentration for all trans-retinal was 80 µM, ten-fold higher than the corresponding Km values of human ALDH1A1 [24], and 5 mM for NAD^+. Fifty mM HEPES at pH 8.0 gave a better performance than PBS buffer solution at pH 7.0 (data not shown).

The RALDH activity was also detected by measuring the fluorescence emitted during the NADH-driven reduction of resazurin to resorufin. Samples obtained from MCF-7 cell monolayers were read in a 96-multiwell plate. The kinetics was evaluated by monitoring the slope obtained during the first 5 min, at a constant temperature of 25 °C, and finally calculated as arbitrary units of fluorescence (AUF) min^{-1} ml^{-1} µg protein. It was also possible to measure RALDH activity using monolayers of triple negative MDA-MB-231 breast cancer cells, although the presence of $ALDH^+$ cells in MDA-MB-231 cells was lower than in MCF-7 cells [9]. Our RALDH assay confirmed these data, since

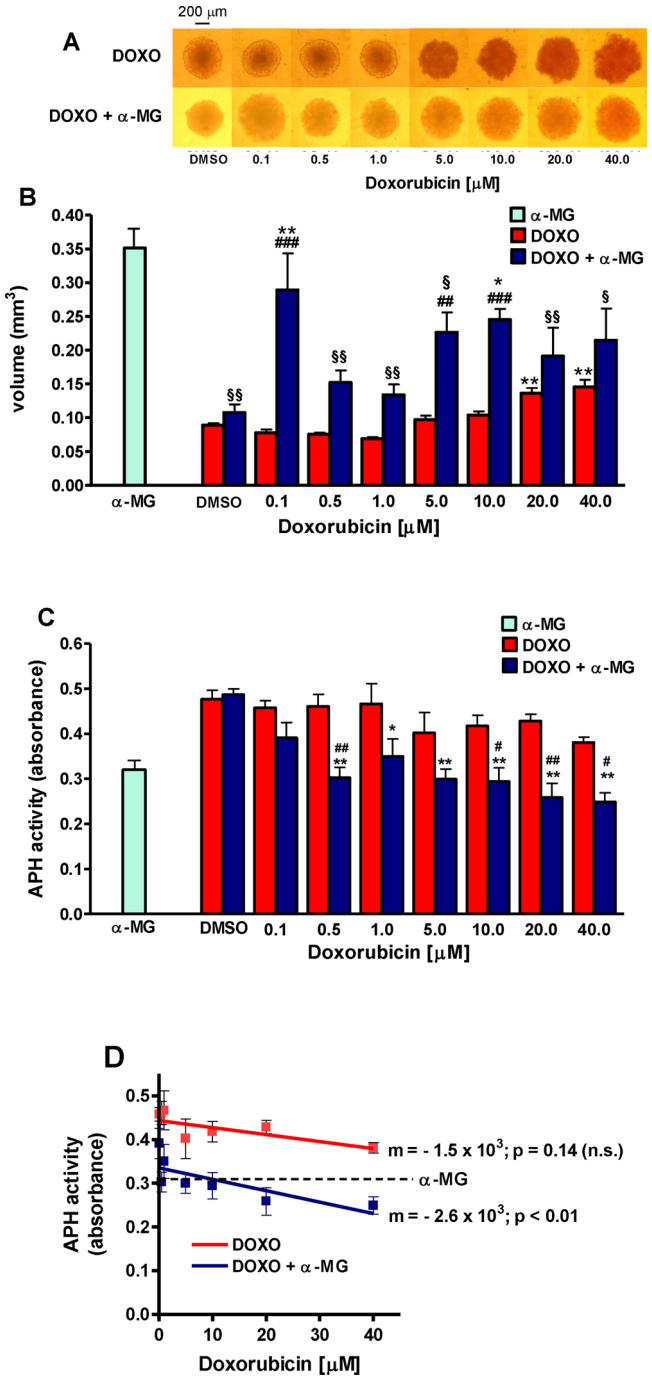

Fig. 3. Morphology and APH activity of MCTSs treated with Doxorubicin or Doxorubicin plus α-MG.

A. The concentrations of Doxorubicin (DOXO) ranged from 0.1–40 μM, both in the presence or absence of 5 μg/ml α-MG. The morphology of MCTSs was not substantially modified by 0.1–1 μM Doxorubicin. Only 5–40 μM Doxorubicin provoked an increasing disaggregation and surface irregularity of MCTSs. However, in the presence of α-MG, the spheroids were partially dissociated at all tested doses of Doxorubicin. B. The volume of MCTSs increased whenever Doxorubicin, alone or in combination with α-MG, caused a spheroid disaggregation. C, D. Doxorubicin, in the range of 0.1–40 μM, provoked a slight decreasing trend of APH activity, although no significant change was observed with respect to control (DMSO) at all doses tested. On the contrary, increasing concentrations of Doxorubicin in the presence of α-MG caused a significant and parallel reduction in APH activity. Values are means ± SEM of at least 4 separate experiments. ANOVA was followed by Dunnett's test for comparisons vs α-MG ($^{§}p < 0.05$ and $^{§§}p < 0.01$) or vs the corresponding untreated values (DMSO) ($^{*}p < 0.05$ and $^{**}p < 0.01$). ANOVA was also followed by Bonferroni's test for comparisons between DOXO and DOXO + α-MG ($^{\#}p < 0.05$ and $^{\#\#}p < 0.01$ vs the corresponding DOXO concentration). The letter m indicates the slope values of the regression lines.

Table 2
IC_{50} of APH activity evaluated in MCTSs after Doxorubicin and α-MG treatment.

	$IC50_{DOXO}$	$IC50_{a\text{-}MG}$	R^2	M/E Ratio
Doxorubicin	50.5 mM		0.93	
α-MG		29.7 μM	0.89	
Doxorubicin + α-MG	8.70 mM		0.87	1.03

The IC_{50} was referred to the APH activity, which represents cell viability, and was calculated after treatment of MCTSs with 0.1–40 μM Doxorubicin, in the presence or absence of 5 μg/ml (12.2 μM) α-MG, or with 0.1–20 μg/ml (0.24–48.6 μM) α-MG. Values of IC_{50} are the means of three independent experiments and R^2 are the corresponding correlation coefficients. The M/E ratio was obtained by treating the MCTSs with Doxorubicin and a-MG together and indicates that the combined administration of the two drugs provided an additive effect on cell death.

the enzyme activity was about five-fold lower in MDA-MB-231 than in MCF-7 cell lysates (Fig. 4B).

This assay was not sufficiently sensitive for single MCTSs and the limit of detection was obtained with a pool of 10 MCF-7 spheroids. However, considering the potential decrement of RALDH activity due to the pharmacological treatment, we always used pools of 40 spheroids. The RALDH activity was about three-fold higher in MCF-7 MCTSs than MCF-7 cell monolayers (Fig. 4C) and a remarkable increase in RALDH activity was also shown in 2 month-old MCF-7 MCTSs with respect to 5 day-old MCF-7 MCTSs (Fig. 4D).

3.5. RT-PCR of ALDH isoenzymes

The quantitative RT-PCR analysis of the ALDH isoenzymes showed that ALDH1A1, ALDH1A3, ALDH1B1, ALDH1L2 and ALDH3A1 were less expressed in MCF-7 MCTSs than MCF-7 cell monolayers. By contrast, the ALDH1A2 expression was unchanged and ALDH2 was more expressed in MCTSs (Fig. 5). The semi-quantitative analysis of the transcripts, evaluated by comparing their Ct values in each sample of cell monolayer or MCTS, showed that the most abundant mRNAs were those of ALDH1A3 and ALDH1B1, whilst ALDH1A1 was the least expressed in both 2D and 3D cell models (Table 3). The expression of ALDH1L1 and ALDH8A1 was too low in all samples and, therefore, was not quantified.

3.6. RALDH activity of MCTSs treated with Doxorubicin and α-MG

Pools of 40 MCF-7 spheroids were treated for 48 h with 5 μg/ml α-MG, or 40 μM Doxorubicin, or the combination of the two drugs at those concentrations (Fig. 6A). Thanks to the fluorescence of Doxorubicin, it was possible to observe its penetration into cells isolated from MCTSs, including dead cells that stained for trypan blue (Fig. 6B).

Compared to control, the RALDH percent activity was blunted in MCTSs after α-MG treatment, whilst in Doxorubicin-treated MCTSs it was increased (Fig. 6C-D). On the contrary, cell viability was decreased after each treatment, as shown by the percentage of APH activity that was lower than control. Doxorubicin plus α-MG provoked an almost complete inhibition of RALDH activity in MCTSs, so that only one sample gave a detectable result, which was extremely lower than control (Fig. 6E). These results were also obtained using MCTSs pooled together in ULA 6-well dishes (data not shown).

4. Discussion

The morphological and morphometric modifications that α-MG and Doxorubicin provoked on MCTSs were very indicative of their toxic effects, especially when they were associated with the reduction in cell viability. Indeed, the first observation of this study is that the increase in volume of the spheroid did not constitute *per se* an evidence of MCTS growth. In fact, the diameter of the spheroid can also depend on the

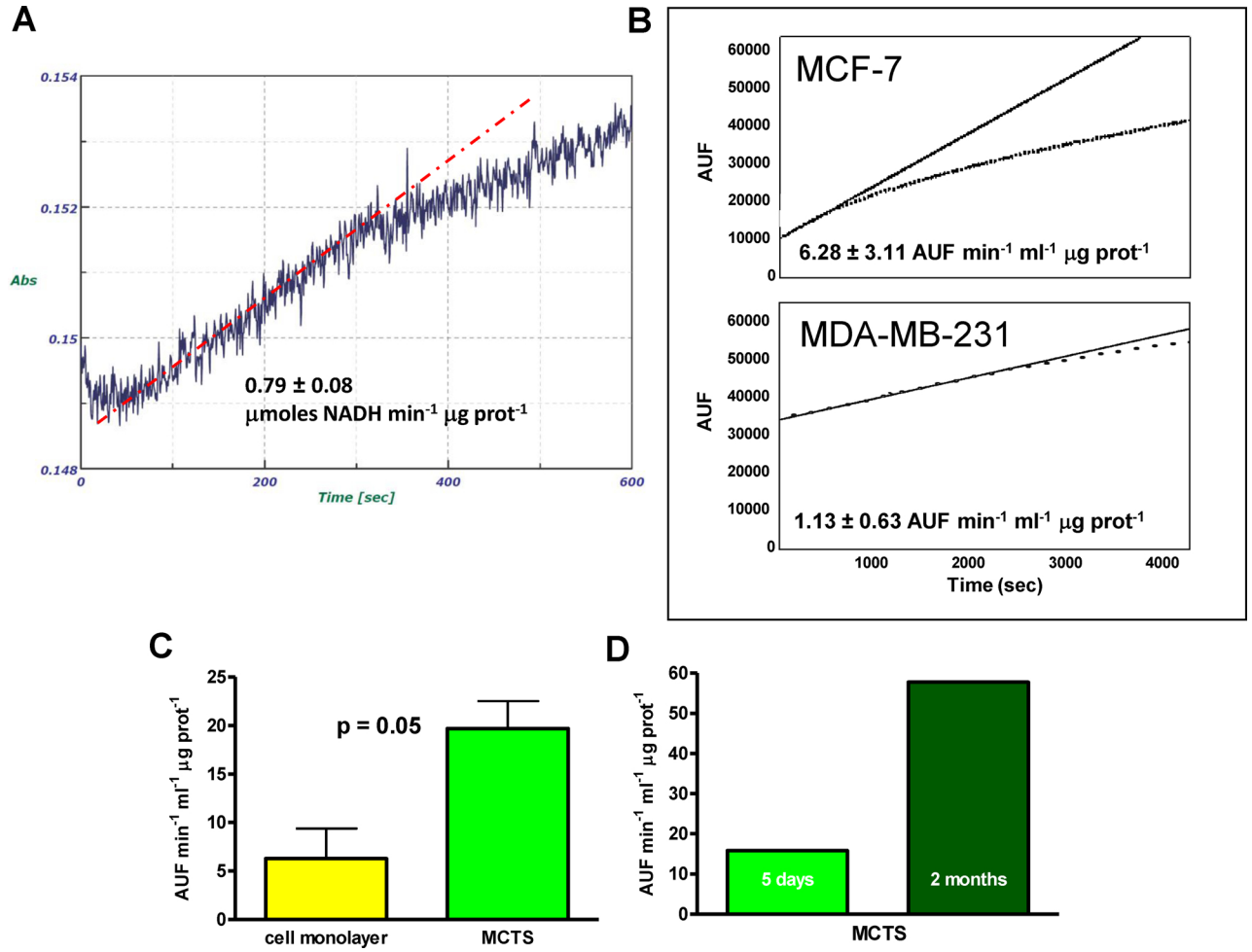

Fig. 4. Characterization of the ALDH activity assay in the presence of retinaldehyde as a substrate.
A. The ALDH used in this assay was that extracted from bread yeast. The slope obtained in the first 5 min (dashed line) was considered representative of RALDH activity. The enzyme activity is expressed as µmoles NADH min^{-1} µg protein of yeast ALDH and is the mean ± SEM of 3 separate experiments. Further details are provided in the Methods section. B. The RALDH activity was also detected by measuring the fluorescence emitted during the NADH-driven reduction of resazurin using 6 × 10^6 MCF-7 and MDA-MB-231 cells, and expressed as means ± SEM of two separated experiments (AUF min^{-1} ml^{-1} µg protein). C. A three-fold higher RALDH activity was measured in pools of 40 MCF-7 MCTSs (n = 3) compared to 6 × 10^6 MCF-7 cells (n = 2). D. The RALDH activity was four-fold higher in 2 month-old MCTSs than in 5 day-old MCTSs.

degree of adhesion that cells establish with one another and with the extracellular matrix. Therefore, if cellular lesions reduce the compactness of the spheroid, the volume increases, the phase contrast density diminishes, and the edge becomes irregular and more jagged. On the contrary, a physiological increase in MCTS volume is due to cell proliferation. In this case, the optical density of the spheroid augments only in the central region, without provoking cell dispersion and modification of its contour. Particular attention should be made when drug concentrations are elevated, since the MCTSs shrink and their density increases homogeneously, also at the periphery. Finally, if under conditions of elevated toxicity the edge is particularly jagged and cells are spared, it can be assumed that there has been a combined effect of cell detachment and cell death. It is noteworthy that all these morphological features are hardly ever highlighted under conditions of high-throughput screenings, since the analyzer is generally limited to measuring only the diameter of the spheroid.

The viability of MCTSs is another relevant parameter for the evaluation of drug toxicity, but it is necessary to use appropriate assays since not all vital dyes enter the core of the spheroids in an effective manner. This is why we adopted the APH assay, as suggested by Friedrich et al., who discussed the failure of other methods to determine cell viability in MCTSs [16].

We initially treated MCTSs with α-MG and Doxorubicin individually and then with the combination of the two drugs, to evaluate whether their toxic effects could add together and the effective doses of Doxorubicin could be reduced. No significant variation of MCTS morphology was observed with α-MG ranging from 0.1 to 1 µg/ml, while 5 µg/ml caused a marked increase in volume. The accompanying lower density and irregularity of the spheroid edge indicated that α-MG provoked a remarkable dissociation of the spheroid. Furthermore, at this dose, a drop in viability of around 40 % also occurred. On the other hand, higher concentrations led to a reduction in the volume of MCTSs, which were homogeneously increased in density, with a certain irregularity of the edge. These morphological lesions were paralleled by a significant reduction in APH activity suggesting that, at these high concentrations, α-MG provokes a sudden reduction in cell viability, shrinking the spheroid without leading to its dissociation. We previously published the morphometric effects of α-MG on MCTSs originated by the MCF-7 cell line, but the variation in their volume and density showed another trend with respect to those described in the present study [15,25]. It is likely that the different number of cells seeded and the increased speed and time of the following centrifugation adopted here to generate MCTSs, was determinant to obtain more compact spheroids with respect to those previously produced. In the present research, the diameter of MCTSs had to be large enough to create a hypoxic environment favoring CSC generation [26]. Therefore,

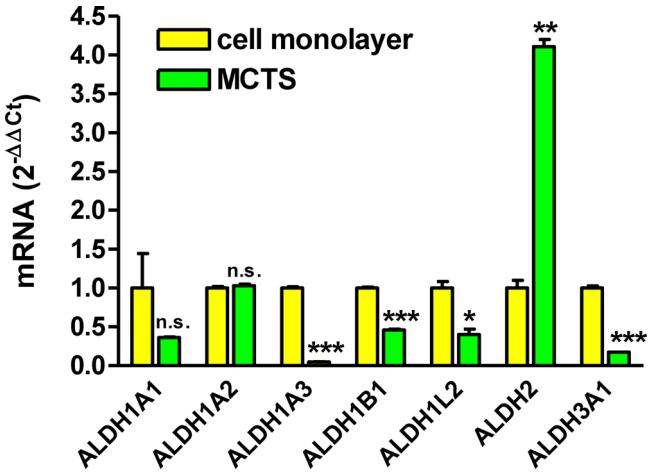

Fig. 5. Quantitative RT-PCR of ALDH isoenzymes evaluated in MCF-7 cell monolayers and MCTSs.

The mRNA expression of the ALDH isoenzymes in MCTSs was quantified by RT-PCR and compared to that obtained in the corresponding cell monolayers, which was normalized to 1.0. The expression of ALDH1A3, ALDH1B1 ALDH1L2 and ALDH3A1 was significantly lower in MCTSs. By contrast, only ALDH2 was more represented in MCTSs. Values are means ± SEM of 2 separate experiments, each obtained in triplicate and analyzed by the Student's t-test. *p < 0.05, **p < 0.01, ***p < 0.001, n.s., not significant vs the corresponding cell monolayer.

Table 3

Comparison of mRNA expression of different ALDH isoenzymes evaluated in cell monolayers and MCTSs.

Gene	Ct	
	cell monolayers	MCTSs
ALDH1A1	35.2	36.2
ALDH1A2	34.5	34.2
ALDH1A3	23.8	27.6
ALDH1B1	24.7	25.5
ALDH1L2	29.2	30.2
ALDH2	31.5	28.8
ALDH3A1	26.5	28.4

The semi-quantitative analysis of the transcripts was performed by comparing the Ct value of each gene. In cell monolayers the decreasing order of expression was 1A3 > 1B1 > 3A1 > 1L2 > 2 > 1A2 > 1A1 and in MCTSs was 1B1 > 1A3 > 3A1 > 2 > 1L2 > 1A2 > 1A1. Values represent means of 2 separate experiments, each obtained in triplicate.

it is conceivable that MCTSs of different sizes and consistency may not be affected by drug treatments in the same way.

Unlike α-MG, the lesions caused by Doxorubicin were much more attenuated, as also shown by its extremely high value of IC_{50}. According to similar investigations performed on MCF-7 spheroids [27–29], the doses of Doxorubicin used in the present research were in the micromolar range. On the contrary, Rama et al. [30] found that nanomolar concentrations of Doxorubicin were toxic for MCF-7 spheroids. A probable reason for this greater drug sensitivity could be the smaller size of the spheroids and the culture conditions that did not support the presence of the resistant subpopulation of CSCs. Compared to α-MG, Doxorubicin provoked a lower disaggregation of MCTSs, while viability was only slightly compromised without reaching a significant difference with vehicle treatment. By contrast, the combination of Doxorubicin with 5 μg/ml α-MG increased the overall cytotoxicity, decreased IC_{50} of Doxorubicin, and led to an additive, but not synergistic, reduction in cell viability. The analysis of the images provided additional information, showing that 5 μg/ml α-MG, at almost all the doses of Doxorubicin, also provoked the expected significant dissociation of MCTSs.

Some possible mechanisms can be suggested to explain how Doxorubicin supported α-MG in reducing cell viability. Doxorubicin inhibits PARP1 and PARP2 and downregulates BRCA1 and BRCA2 in MCF-7 cells [31]. These enzymes protect cells from DNA injury by activating the process of DNA repair [32]. Therefore, their reduced activity could amplify the cell damaged caused by α-MG in MCF-7 MCTSs. Moreover, both Doxorubicin and α-MG exert a remarkable inhibition on topoisomerase II in mammalian proliferating cells, leading to cytotoxic effects [33,34]. Doxorubicin acts by an indirect mechanism on topoisomerase II, since it intercalates DNA and forms a ternary complex with the enzyme. This provokes double-strand breaks and transcriptional modification, especially in rapidly dividing cancer cells, that in turn lead to cell apoptosis [35]. α-MG could reinforce this effect because it also suppresses topoisomerase II, but without stabilizing a topoisomerase II-DNA complex, since it binds the enzyme more directly [34].

Thanks to the reduction of the effective dose of Doxorubicin, the presumable clinical advantage of the contemporary administration of the two drugs is that healthy tissues, with particular regard to the heart and brain, which are the preferred targets of antracyclins [36], can be more preserved in long-term treatments. It has also been demonstrated that α-MG can exert a cardioprotective action by reducing apoptotic death and ROS-dependent damages in cardiomyocytes subjected to oxidative stress [37]. Moreover, micromolar concentrations of α-MG protect the ischemic heart from the reperfusion injury [38]. Interestingly, it has been shown that some xanthones extracted from Garcinia Mangostana reduced the side effects caused by Doxorubicin in the central nervous system [39] and doses of 10–20 μM α-MG administered for 48 h were not harmful for isolated hepatocytes [40]. Finally, we previously demonstrated that the dissociation caused by α-MG on spheroids generated by an MDA-MB-231 breast cancer cell line did not increase cell migration [15], and Wang et al. showed that this xanthone can even exert an anti-invasive action [41].

The degree of toxicity exerted by α-MG and Doxorubicin on bulk cells was then compared with the damage that the drugs caused to cells that were characterized by an increased RALDH activity. In particular, ALDH1A1 and ALDH1A3 have been invoked as markers of CSCs, especially in luminal breast cancers [7]. The method most commonly used to quantify cells with increased ALDH activity is a flow cytometry analysis that uses a specific substrate for this dehydrogenase superfamily [42]. However, this assay is hampered by the limitation of not distinguishing among the ALDH isoenzymes, since neither the substrate nor the inhibitor used are specific for the ALDH1 or other isoforms [43–45]. The assay characterized in the present research instead discriminates the subfamily of ALDH1, whose preferential substrate is all-trans retinal, but not ALDH8A1 (or ALDH12), which oxidizes only 9-cis-retinal [46]. Other ALDH isoenzymes have greater affinity for substrates different from retinal, such as ALDH1L1 and ALDH1L2, which use one carbon aldehyde in the folate pathway [47], ALDH2, which catalyzes acetaldehyde oxidation, and ALDH3, which converts aromatic aldehydes [48]. Furthermore, the sensitivity of our assay is comparable to that of other fluorimetric methods that measure total ALDH activity. However, we needed to group together several spheroids or grow and collect them in a single plate to obtain sufficiently detectable activity after pharmacological treatments.

The mRNA expression of ALDH1A3 and ALDH1B1 was the highest, whilst that of ALDH1A1 was the least abundant, in both cell monolayers and MCTSs. These results agree with literature data that indicate, among the ALDH gene family, ALDH1A3 as the most expressed in breast carcinoma stem cells [9,49] and ALDH1B1 as the only isoenzyme that significantly increases in luminal breast cancer [50]. In addition to its biomarker properties, Croker et al. also underlined a regulatory role for ALDH1A3, since its knockdown decreased CFU-F formation and metastases in human breast cancer cells [51]. Moreover, only knocking down ALDH1A3, but not ALDH1A1, led to a decrease in ALDH activity. A functional role was also demonstrated for ALDH1B1, because it exerts a drug detoxifying action [50] and shows a high affinity not only for retinaldehyde but also for acetaldehyde [52]. By contrast, ALDH1A1

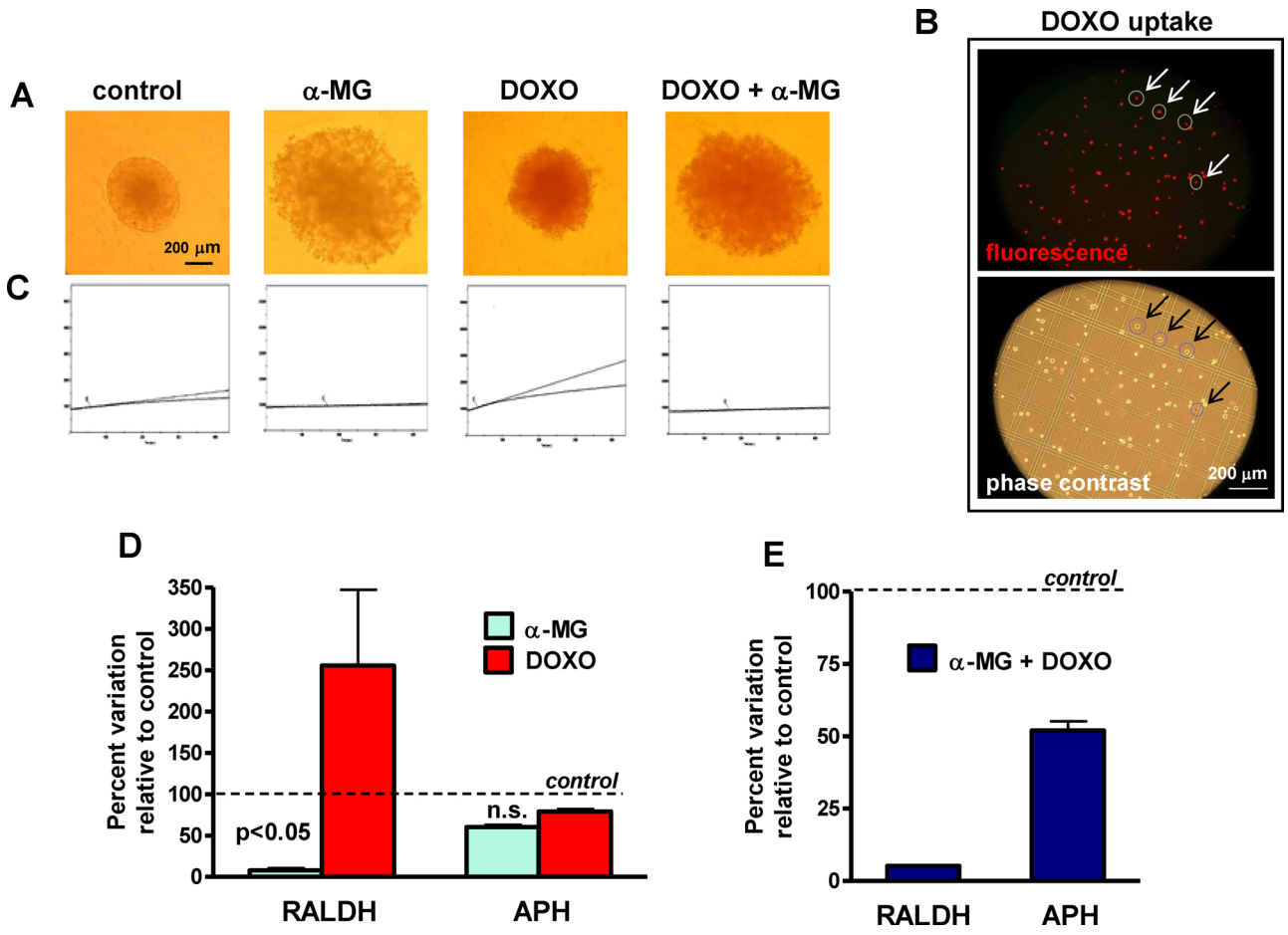

Fig. 6. Effect of α-MG and Doxorubicin on RALDH activity evaluated in MCTSs.
A. The micrographs show the changes in MCTS morphology due to the treatment with 5 μg/ml α-MG (α-MG), 40 μM Doxorubicin (DOXO), and their combination (DOXO + α-MG). B. Cell uptake of Doxorubicin is shown by the red color emission due to the intrinsic fluorescence of the drug. The trypan blue staining indicates dead cells (arrows). C. Pools of 40 spheroids were used to measure RALDH kinetics according to the fluorescence assay described in the Methods section. Compared to control, the slopes of α-MG and DOXO + α-MG samples were extremely lower, whilst that of DOXO samples was more accentuated. D. The percentage of RALDH activity compared to control (100 %) was significantly lower in α-MG (7.61 ± 2.92, n = 2) than in DOXO samples (255.6 ± 91.9, n = 3). By contrast, there were no significant differences (n.s.) between the percentages of APH activities (n = 4) in α-MG and DOXO samples (60.2 ± 2.69 and 79.3 ± 2.96, respectively; values are means ± SEM analyzed by the Student's t-test). E. Only one sample of DOXO + α-MG gave a detectable RALDH activity, whose percentage was 5.21 compared to control. The combined treatment also led to a marked reduction in APH activity, whose percentage was 52.0 ± 3.19 compared to control (n = 4).

was the least expressed in both our cell culture models, confirming the findings of Shen et al. showing that this isoenzyme is less represented than ALDH1A3 in breast cancer [53]. Furthermore, the mRNA expression of ALDH1A1, ALDH1A2 and ALDH1A3, which was deduced by these authors by analyzing the ONCOMINE gene expression array database, were downregulated in breast cancer cells when compared to normal tissue. Nevertheless, whether an increase or decrease in distinct ALDH isoenzyme expression really occurs in breast cancer is still under debate, as reported, for example, by the Kaplan-Meier plotter database analysis [54] that shows a different behavior of breast cancer RALDH isoenzymes with respect to the ONCOMINE database.

By comparing the 2D vs 3D cell model, in the present study we showed a lower expression of ALDH1A1, ALDH1A3, ALDH1B1 and ALDH1L2 in MCTSs than cell monolayers. Only ALDH2 was more expressed in MCTSs, whilst ALDH1A2 did not change in the passage from the 2D to 3D cell culture model. Hence, these findings are in contrast with the opposite trend of the RALDH activity, revealed by our fluorimetric assay, which was higher in MCTSs than cell monolayers. This observed increase in catalytic activity, which was paralleled by the downregulation of the enzyme expression, might be justified by a covalent activation of the existent molecules. Di Zao et al. showed that, in breast CSCs, the deacetylation of ALDH1A1 in lysine 353 increased its enzyme activity [55]. This process started with Notch involvement that induced the cytoplasmic deacetylase sirtuin-2, thus increasing ALDH1A1 activity and the self-renewal of CSCs [55]. Notably, Sansone et al. showed that the activity of the stem cell regulatory gene Notch-3 in MCF-7 mammospheres was more elevated under hypoxia conditions [56]. This pathway was supported by the binding of HIF-1α at the level of the Notch-responsive promoters, which maintains stem cells in an undifferentiated state [57]. The role of hypoxia in stimulating ALDH in the spheroids was also revealed by the higher activity of RALDH that we measured in 2-month-old MCTSs, whose size, and presumably hypoxic core, was markedly increased with respect to the 5-day-old MCTSs.

Concerning the pharmacological effects investigated in this study, we found that α-MG exerted a significant inhibition of the RALDH activity in MCTSs since its activity dropped to 7 %, despite the presence of 60 % viable cells. α-MG provoked the dissociation of the spheroid and this presumably hampered cell-to-cell interactions and, therefore, the binding of Jagged/Delta to the Notch receptor, leading to sirtuin-2 downregulation and inhibition of RALDH activity [55]. Indeed, the administration of an antibody that halted Jagged-1/Notch-3 binding reduced the self-renewal of MCF-7 stem cells expanded as multicellular spheroids, indicating that Notch-3 acted through a canonical ligand-receptor interaction [56]. This was further demonstrated by the same authors who showed that the formation of MCF-7 spheroids was extremely reduced when MCF-7 cells were transfected with a Jagged-1

specific siRNA [58]. Moreover, it was also shown that α-MG inhibited the Notch signaling pathway by reducing the activity of γ-secretase with an IC_{50} value of 8.0 μM [59], a concentration similar to that we used in the present study (12.2 μM) to inhibit RALDH activity. The underlying mechanism of γ-secretase inhibition seems to be referred to an increased degradation of nicastrin, one of the four subunits of this enzyme, a process that was demonstrated using the α-MG analogue cowanin [59]. In particular, it was suggested that these hydrophobic xantones preferentially bind the immature, not-glycosylated, form of nicastrin, thus impeding its following interaction with the subunit PS1. This might lead to an increased instability of nicastrin and its accelerated degradation [59].

Another mechanism underlying the α-MG-dependent decrease in RALDH activity could be the blunting effects induced by this drug on STAT3, since a positive correlation between the phosphorylated/activated form of STAT3 and ALDH1 expression has been observed in breast CSCs [60]. Hafeez et al. showed that micromolar concentrations of α-MG inhibited STAT3 activity by blocking its phosphorylation in Ser737/Tyr705 and by reducing its binding to DNA [61]. Similarly, Shan et al. demonstrated that α-MG suppressed gastric adenocarcinoma cell lines via blockade of STAT3 signaling pathway [62]. Hence, α-MG, via STAT3 inhibition, could have decreased ALDH1 expression and consequently reduced RALDH activity in MCTSs.

In contrast to α-MG, Doxorubicin exerted an opposite effect in MCTSs by increasing RALDH activity. STAT3 could be still involved, because several reports show that the increased resistance to Doxorubicin of MCF-7, as well as other breast cancer cell lines, was mediated by the overexpression of both STAT3 and ALDH1 [60,63,64]. In this regard, Croker et al. abolished breast cancer cell resistance to Doxorubicin by using some inhibitors of ALDH activity, underlining the primary role of this dehydrogenase in determining the cell insensitivity to this chemotherapeutic drug [65].

On the basis of the data reported above, we suggest a possible scenario in which α-MG could inhibit STAT3 phosphorylation in MCTSs and, in turn, abolish the effects of the Doxorubicin-dependent overexpression of STAT3 on ALDH induction. Moreover, to explain how Doxorubicin also supported the α-MG-operated reduction of RALDH activity, we speculate that α-MG, through STAT3 inhibition, could have allowed Doxorubicin to provoke injuries also to $ALDH^+$ CSCs, thus reducing their abundance in the MCTSs. This hypothesis is in agreement with the recent report of Liu et al. indicating that the overexpression of STAT3 observed in MCF-7 CSCs was correlated to their resistance to Doxorubicin and that the inability of this drug to affect CSCs was reversed by silencing STAT3 [66].

5. Conclusions

A new and simple assay of RALDH activity has been proposed to evaluate a subpopulation of stem cells that is most frequently present in luminal breast cancers. Our findings provided evidence that the combined administration of Doxorubicin and α-MG to MCF-7 spheroids significantly decreased cell viability and RALDH activity, thus reversing both bulk and stem cell resistance to Doxorubicin.

Availability of data and materials

Data of interest will be made available on request.

Funding

Funding for this research was obtained from the University of Bologna, Italy.

Declaration of Competing Interest

The authors declare that there are no conflicts of interest.

References

[1] Á. Fábián, G. Vereb, J. Szöllősi, The hitchhikers guide to cancer stem cell theory: markers, pathways and therapy, Cytometry A. 83 (2013) 62–71.
[2] S.D. Mertins, Cancer stem cells: a systems biology view of their role in prognosis and therapy, Anticancer Drugs 25 (2014) 353–367.
[3] S. Palomeras, S. Ruiz-Martínez, T. Puig, Targeting breast Cancer stem cells to overcome treatment resistance, Molecules (2018), https://doi.org/10.3390/molecules23092193.
[4] B. Jackson, C. Brocker, D.C. Thompson, W. Black, K. Vasiliou, D.W. Nebert DW, V. Vasiliou, Update on the aldehyde dehydrogenase gene (ALDH) superfamily, Hum. Genomics 5 (2011) 283–303.
[5] L. Dollé, L. Boulter, I.A. Leclercq, L.A. van Grunsven, Next generation of ALDH substrates and their potential to study maturational lineage biology in stem and progenitor cells, Am. J. Physiol. Gastrointest. Liver Physiol. 308 (2015) G573–G578.
[6] D. Raha, T.R. Wilson, J. Peng, D. Peterson, P. Yue, M. Evangelista, C. Wilson, M. Merchant, J. Settleman, The cancer stem cell marker aldehyde dehydrogenase is required to maintain a drug-tolerant tumor cell subpopulation, Cancer Res. 74 (2014) 3579–3590.
[7] S. Liu, Y. Cong, D. Wang, Y. Sun, L. Deng, Y. Liu, R. Martin-Trevino, L. Shang, S.P. McDermott, M.D. Landis, S. Hong, A. Adams, R. D'Angelo, C. Ginestier, E. Charafe-Jauffret, S.G. Clouthier, D. Birnbaum, S.T. Wong, M. Zhan, J.C. Chang, M.S. Wicha, Breast cancer stem cells transition between epithelial and mesenchymal states reflective of their normal counterparts, Stem Cell Reports 2 (2013) 78–91.
[8] P. Marcato, C.A. Dean, C.A. Giacomantonio, P.W. Lee, Aldehyde dehydrogenase: its role as a cancer stem cell marker comes down to the specific isoform, Cell Cycle 10 (2011) 1378–1384.
[9] P. Marcato, C.A. Dean, D. Pan, R. Araslanova, M. Gillis, M. Joshi, L. Helyer, L. Pan, A. Leidal, S. Gujar, C.A. Giacomantonio, P.W.K. Lee, Aldehyde dehydrogenase activity of breast cancer stem cells is primarily due to isoform ALDH1A3 and its expression is predictive of metastasis, Stem Cells 29 (2011) 32–45.
[10] G. Chen, Y. Li, W. Wang, L. Deng, Bioactivity and pharmacological properties of α-mangostin from the mangosteen fruit: a review, Expert Opin. Ther. Pat. 28 (2018) 415–427.
[11] A.M. Meredith, C.R. Dass, Increasing role of the cancer chemotherapeutic doxorubicin in cellular metabolism, J. Pharm. Pharmacol. 68 (2016) 729–741.
[12] M.Songbo H. Lang, C. Xinyong, X. Bin, Z. Ping, S. Liang, Oxidative stress injury in doxorubicin-induced cardiotoxicity, Toxicol. Lett. 307 (2019) 41–48.
[13] N. Koleini, B.E. Nickel, A.L. Edel, R.R. Fandrich, A. Ravandi, E. Kardami, Oxidized phospholipids in Doxorubicin-induced cardiotoxicity, Chem. Biol. Interact. 303 (2019) 35–39.
[14] E.F. Silva, R.F. Bazoni, E.B. Ramos, M.S. Rocha, DNA-doxorubicin interaction: new insights and peculiarities, Biopolymers (2017), https://doi.org/10.1002/bip.22998.
[15] G. Scolamiero, C. Pazzini, F. Bonafè, C. Guarnieri, C. Muscari, Effects of α-Mangostin on viability, growth and cohesion of multicellular spheroids derived from human breast Cancer cell lines, Int. J. Med. Sci. 15 (2018) 23–30.
[16] J. Friedrich, W. Eder, J. Castaneda, M. Doss, E. Huber, R. Ebner, L.A. Kunz-Schughart, A reliable tool to determine cell viability in complex 3-d culture: the acid phosphatase assay, J. Biomol. Screen. 12 (2007) 925–937.
[17] T.C. Chou, Theoretical basis, experimental design, and computerized simulation of synergism and antagonism in drug combination studies, Pharmacol. Rev. 58 (2006) 621–681.
[18] T.C. Chou, Drug combination studies and their synergy quantification using the Chou-Talalay method, Cancer Res. 70 (2010) 440–446.
[19] A. Papi, S. De Carolis, S. Bertoni, G. Storci, V. Sceberras, D. Santini, C. Ceccarelli, M. Taffurelli, M. Orlandi, M. Bonafé, PPARγ and RXR ligands disrupt the inflammatory cross-talk in the hypoxic breast cancer stem cells niche, J. Cell. Physiol. 229 (2014) 1595–1606.
[20] M.M. Bradford, A rapid and sensitive method for the quantitation of microgram quantities of protein utilizing the principle of protein-dye binding, Anal. Biochem. 72 (1976) 248–254.
[21] K.J. Livak, T.D. Schmittgen, Analysis of relative gene expression data using real-time quantitative PCR and the 2(-Delta Delta C(T)) method, Methods. 25 (2001) 402–408.
[22] X. Liu, J. Xie, Z. Liu, Q. Gong, R. Tian, G. Su, Identification and validation of reference genes for quantitative RT-PCR analysis of retinal pigment epithelium cells under hypoxia and/or hyperglycemia, Gene 580 (2016) 41–46.
[23] R.Z. Lin, H.Y. Chang, Recent advances in three-dimensional multicellular spheroid culture for biomedical research, Biotechnol. J. 3 (2008) 1172–1184.
[24] R. Bchini, V. Vasiliou, G. Branlant, F. Talfournier, S. Rahuel-Clermont, Retinoic acid biosynthesis catalyzed by retinal dehydrogenases relies on a rate-limiting conformational transition associated with substrate recognition, Chem. Biol. Interact. 202 (2013) 78–84.
[25] F. Bonafè, C. Pazzini, S. Marchionni, C. Guarnieri, C. Muscari, Complete disaggregation of MCF-7-derived breast tumour spheroids with very low concentrations of α-Mangostin loaded in CD44 thioaptamer-tagged nanoparticles, Int. J. Med. Sci. 16 (2019) 33–42.
[26] A. Shiraishi, K. Tachi, N. Essid, I. Tsuboi, M. Nagano, T. Kato, T. Yamashita, H. Bando, H. Hara, O. Ohneda, Hypoxia promotes the phenotypic change of aldehyde dehydrogenase activity of breast cancer stem cells, Cancer Sci. 108 (2017) 362–372.
[27] T.M. Sun, Y.C. Wang, F. Wang, J.Z. Du, C.Q. Mao, C.Y. Sun, R.Z. Tang, Y. Liu, J. Zhu, Y.H. Zhu, X.Z. Yang, J. Wang, Cancer stem cell therapy using doxorubicin

conjugated to gold nanoparticles via hydrazone bonds, Biomaterials. 35 (2014) 836–845.
[28] W. Zhang, C. Li, B.C. Baguley, F. Zhou, W. Zhou, J.P. Shaw, Z. Wang, Z. Wu, J. Liu, Optimization of the formation of embedded multicellular spheroids of MCF-7 cells: how to reliably produce a biomimetic 3D model, Anal. Biochem. 515 (2016) 47–54.
[29] R. Akasov, M. Drozdova, D. Zaytseva-Zotova, M. Leko, P. Chelushkin, A. Marc, I. Chevalot, S. Burov, N. Klyachko, T. Vandamme, E. Markvicheva, Novel doxorubicin derivatives: synthesis and cytotoxicity study in 2D and 3D in vitro models, Adv. Pharm. Bull. 7 (2017) 593–601.
[30] A.R. Rama, J. Prados, C. Melguizo, M. Burgos, P.J. Alvarez, F. Rodriguez-Serrano, J.L. Ramos, A. Aranega, Synergistic antitumoral effect of combination E gene therapy and Doxorubicin in MCF-7 breast cancer cells, Biomed. Pharmacother. 65 (2011) 260–270.
[31] J.O. Tun, L.A. Salvador-Reyes, M.C. Velarde, N. Saito, K. Suwanborirux, G.P. Concepcion, Synergistic cytotoxicity of renieramycin m and doxorubicin in MCF-7 breast Cancer cells, Mar. Drugs (2019), https://doi.org/10.3390/md17090536.
[32] S.M. Noordermeer, H. van Attikum, PARP inhibitor resistance: a tug-of-War in BRCA-Mutated cells, Trends Cell Biol. 29 (2019) 820–834.
[33] F.A. Fornari, J.K. Randolph, J.C. Yalowich, M.K. Ritke, D.A. Gewirtz, Interference bydoxorubicin with DNA unwinding in MCF-7 breast tumor cells, Mol. Pharmacol. 45 (1994) 649–656.
[34] Y. Mizushina, I. Kuriyama, T. Nakahara, Y. Kawashima, H. Yoshida, Inhibitory effects of α-mangostin on mammalian DNA polymerase, topoisomerase, and human cancer cell proliferation, Food Chem. Toxicol. 59 (2013) 793–800.
[35] C.G. Tocchetti, C. Cadeddu, D. Di Lisi, S. Femminò, R. Madonna, D. Mele, I. Monte, G. Novo, C. Penna, A. Pepe, P. Spallarossa, G. Varricchi, C. Zito, P. Pagliaro, G. Mercuro, From molecular mechanisms to clinical management of antineoplastic drug-induced cardiovascular toxicity: a translational overview, Antioxid. Redox Signal. 30 (2019) 2110–2153.
[36] C. Carvalho, R.X. Santos, S. Cardoso, S. Correia, P.J. Oliveira, M.S. Santos, P.I. Moreira, Doxorubicin: the good, the bad and the ugly effect, Curr. Med. Chem. 16 (2009) 3267–3285.
[37] Z. Fang, W. Luo, Y. Luo, Protective effect of α-mangostin against CoCl2-induced apoptosis by suppressing oxidative stress in H9C2 rat cardiomyoblasts, Mol. Med. Rep. 17 (2018) 6697–6704.
[38] M. Buelna-Chontal, F. Correa, S. Hernández-Reséndiz, C. Zazueta, J. Pedraza-Chaverri, Protective effect of α-mangostin on cardiac reperfusion damage by attenuation of oxidative stress, J. Med. Food 14 (2011) 1370–1374.
[39] J. Tangpong, S. Miriyala, T. Noel, C. Sinthupibulyakit, P. Jungsuwadee, D.K. St Clair, Doxorubicin-induced central nervous system toxicity and protection by xanthone derivative of Garcinia mangostana, Neuroscience. 175 (2011) 292–299.
[40] S.C. Hsieh, M.H. Huang, C.W. Cheng, J.H. Hung, S.F. Yang, Y.H. Hsieh, α-Mangostin induces mitochondrial dependent apoptosis in human hepatoma SK-Hep-1 cells through inhibition of p38 MAPK pathway, Apoptosis 18 (2013) 1548–1560.
[41] J.J. Wang, B.J. Sanderson, W. Zhang, Significant anti-invasive activities of α-mangostin from the mangosteen pericarp on two human skin cancer cell lines, Anticancer Res. 32 (2012) 3805–3816.
[42] L. Mele, D. Liccardo, V. Tirino, Evaluation and isolation of Cancer stem cells using ALDH activity assay, Methods Mol. Biol. 1692 (2018) 43–48.
[43] J.S. Moreb, D. Ucar, D.S. Han, J.K. Amory, A.S. Goldstein, B. Ostmark, L.J. Chang, The enzymatic activity of human aldehyde dehydrogenases 1A2 and 2 (ALDH1A2 and ALDH2) is detected by Aldefluor, inhibited by diethylaminobenzaldehyde and has significant effects on cell proliferation and drug resistance, Chem. Biol. Interact. 195 (2012) 52–60.
[44] L. Zhou, D. Sheng, D. Wang, W. Ma, Q. Deng, L. Deng, S. Liu, Identification of cancer-type specific expression patterns for active aldehyde dehydrogenase (ALDH) isoforms in ALDEFLUOR assay, Cell Biol. Toxicol. 35 (2019) 161–177.
[45] C.A. Morgan, B. Parajuli, C.D. Buchman, K. Dria, T.D. Hurley, N,N-diethylaminobenzaldehyde (DEAB) as a substrate and mechanism-based inhibitor for human ALDH isoenzymes, Chem. Biol. Interact. 234 (2015) 18–28.
[46] I. Davis, Y. Yang, D. Wherritt, A. Liu, Reassignment of the human aldehyde dehydrogenase ALDH8A1 (ALDH12) to the kynurenine pathway in tryptophan catabolism, J. Biol. Chem. 293 (2018) 9594–9603.
[47] S.A. Krupenko, N.I. Krupenko, ALDH1L1 and ALDH1L2 Folate Regulatory Enzymes in Cancer, Adv. Exp. Med. Biol. 1032 (2018) 127–143.
[48] A. Yoshida, A. Rzhetsky, L.C. Hsu, C. Chang, Human aldehyde dehydrogenase gene family, Eur. J. Biochem. 251 (1998) 549–557.
[49] X. Bai, J. Ni, J. Beretov, P. Graham, Y. Li, Cancer stem cell in breast cancer therapeutic resistance, Cancer Treat. Rev. 69 (2018) 152–163.
[50] T.S. Gerashchenko, E.V. Denisov, N.M. Novikov, L.A. Tashireva, E.V. Kaigorodova, O.E. Savelieva, M.V. Zavyalova, N.V. Cherdyntseva, V.M. Perelmuter, Different morphological structures of breast tumors demonstrate individual drug resistance gene expression profiles, Exp. Oncol. 40 (2018) 228–234.
[51] A.K. Croker, M. Rodriguez-Torres, Y. Xia, S. Pardhan, H.S. Leong, J.D. Lewis, A.L. Allan, Differential functional roles of ALDH1A1 and ALDH1A3 in mediating metastatic behavior and therapy resistance of human breast Cancer cells, Int. J. Mol. Sci. (2017), https://doi.org/10.3390/ijms18102039.
[52] S. Singh, J. Arcaroli, Y. Chen, D.C. Thompson, W. Messersmith, A. Jimeno, V. Vasiliou, ALDH1B1 is crucial for Colon tumorigenesis by modulating wnt/β-Catenin, notch and PI3K/Akt signaling pathways, PLoS One (2015), https://doi.org/10.1371/journal.pone.0121648.
[53] J.X. Shen, J. Liu, G.W. Li, Y.T. Huang, H.T. Wu HT, Mining distinct aldehyde dehydrogenase 1 (ALDH1) isoenzymes in gastric cancer, Oncotarget. 7 (2016) 25340–25349.
[54] S. Wu, W. Xue, X. Huang, X. Yu, M. Luo, Y. Huang, Y. Liu, Z. Bi, X. Qiu, S. Bai, Distinct prognostic values of ALDH1 isoenzymes in breast cancer, Tumour Biol. 36 (2015) 2421–2426.
[55] D. Zhao, Y. Mo, M.T. Li, S.W. Zou, Z.L. Cheng, Y.P. Sun, Y. Xiong, K.L. Guan, Q.Y. Lei, NOTCH-induced aldehyde dehydrogenase 1A1 deacetylation promotes breast cancer stem cells, J. Clin. Invest. 124 (2014) 5453–5465.
[56] P. Sansone, G. Storci, C. Giovannini, S. Pandolfi, S. Pianetti, M. Taffurelli, D. Santini, C. Ceccarelli, P. Chieco, M. Bonafé, p66Shc/Notch-3 interplay controls self-renewal and hypoxia survival in human stem/progenitor cells of the mammary gland expanded in vitro as mammospheres, Stem Cells 25 (2007) 807–815.
[57] M.V. Gustafsson, X. Zheng, T. Pereira, K. Gradin, S. Jin, J. Lundkvist, L. Ruas, L. Poellinger, U. Lendahl, M. Bondesson, Hypoxia requires notch signaling to maintain the undifferentiated cell state, Dev. Cell 9 (2005) 617–628.
[58] P. Sansone, G. Storci, S. Tavolari, T. Guarnieri, C. Giovannini, M. Taffurelli, C. Ceccarelli, D. Santini, P. Paterini, K.B. Marcu, P. Chieco, M. Bonafé, IL-6 triggers malignant features in mammospheres from human ductal brest carcinoma and normal mammary gland, J. Clin. Invest. 117 (2007) 3988–4002.
[59] M.A. Arai, R. Akamine, A. Tsuchiya, T. Yoneyama, T. Koyano, T. Kowithayakorn, M. Ishibashi, The Notch inhibitor cowanin accelerates nicastrin degradation, Sci. Rep. (2018), https://doi.org/10.1038/s41598-018-23698-4.
[60] L. Lin, B. Hutzen, H.F. Lee, Z. Peng, W. Wang, C. Zhao, H.J. Lin, D. Sun, P.K. Li, C. Li, H. Korkaya, M.S. Wicha, J. Lin, Evaluation of STAT3 signaling in ALDH+ and ALDH+/CD44+/CD24- subpopulations of breast cancer cells, PLoS One (2013), https://doi.org/10.1371/journal.pone.0082821.
[61] B.B. Hafeez, A. Mustafa, J.W. Fischer, A. Singh, W. Zhong, M.O. Shekhani, L. Meske, T. Havighurst, K. Kim, A.K. Verma, α-Mangostin: a dietary antioxidant derived from the pericarp of Garcinia mangostana L. inhibits pancreatic tumor growth in xenograft mouse model, Antioxid. Redox Signal. 21 (2014) 682–699.
[62] T. Shan, X.J. Cui, W. Li, W.R. Lin, H.W. Lu, Y.M. Li, X. Chen, T. Wu, α-Mangostin suppresses human gastric adenocarcinoma cells in vitro via blockade of Stat3 signaling pathway, Acta Pharmacol. Sin. 35 (2014) 1065–1073.
[63] M.P. Moreira, L. da Conceição Braga, G.D. Cassali, L.M. Silva, STAT3 as a promising chemoresistance biomarker associated with the CD44(+/high)/CD24(-/low)/ALDH(+) BCSCs-like subset of the triple-negative breast cancer (TNBC) cell line, Exp. Cell Res. 363 (2018) 283–290.
[64] D. Jia, Y. Tan, H. Liu, S. Ooi, L. Li, K. Wright, S. Bennett, C.L. Addison, L. Wang, Cardamonin reduces chemotherapy-enriched breast cancer stem-like cells in vitro and in vivo, Oncotarget. 7 (2016) 771–785.
[65] A.K. Croker, A.L. Allan, Inhibition of aldehyde dehydrogenase (ALDH) activity reduces chemotherapy and radiation resistance of stem-like $ALDH^{hi}CD44^{+}$ human breast cancer cells, Breast Cancer Res. Treat. 133 (2012) 75–87.
[66] C. Liu, H. Xing, C. Guo, Z. Yang, Y. Wang, Y. Wang, MiR-124 reversed the doxorubicin resistance of breast Cancer stem cells through STAT3/HIF-1 signaling pathways, Cell Cycle (2019), https://doi.org/10.1080/15384101.2019.1638182.